Research article

Minjie Fang[a], Sihui Huang[a], Dong Li, Chunli Jiang, Pei Tian, Hechun Lin, Chunhua Luo*, Wenlei Yu and Hui Peng*

Stretchable and self-healable organometal halide perovskite nanocrystal-embedded polymer gels with enhanced luminescence stability

https://doi.org/10.1515/nanoph-2018-0126
Received August 26, 2018; revised October 15, 2018; accepted October 15, 2018

Abstract: Stretchable and self-healing polymer gels with luminescent property are very promising materials for next generation soft optical devices. This work presents the preparation of self-healing and luminescent polymer gels by simply blending organometal halide perovskite nanocrystals (OHP NCs) with poly(dimethylsiloxane)-urea copolymer (PDMS-urea). On the one hand, the obtained luminescent gels are not only flexible, stretchable and relatively transparent, they also exhibit excellent self-healing capability due to the reversible hydrogen bonding network in the PDMS-urea copolymer. On the other hand, the embedding of OHP NCs ($MAPbBr_3$ and $MAPbI_3$ NCs) inside the hydrophobic PDMS-urea gel greatly improved the photoluminescence stability of OHP NCs against water. Their applications as phosphors for LEDs have been demonstrated. Both the $MAPbBr_3$/PDMS-urea gel and $MAPbI_3$/PDMS-urea gel can fully convert the blue emission of GaN chip to green and red emissions, respectively. These gels can be used as photoluminescent materials in flexible optical devices with good self-healing capability.

Keywords: luminescent; organometal halide perovskite nanocrystals; poly(dimethylsiloxane)-urea gel; self-healable; soft optical devices.

1 Introduction

Over the past few years, organometal halide perovskite nanocrystals (OHP NCs) have received great interest because of their unique properties, such as high photoluminescence efficiency, tunable emission wavelength in the visible light region, narrow emission bandwidth and easy processability [1–3]. This makes perovskite NCs very promising photoelectronic materials in light-emitting diodes, NC lasers and solar cells [4–6]. However, the inferior stability of HP NCs, which are moisture- and air-sensitive, has set a great challenge to their practical applications [7, 8]. To address the stability issue, a variety of methods, including protective coating [9, 10], alternative capping ligands other than oleic acid (OA)/oleylamine (OLAm) [11, 12] and polymer blends [13–16], have been employed with significant success achieved. For example, Huang's group reported the improved stability of $MAPbBr_3$ NCs through the protective coating of silica oxide [10]. Wang et al. utilised an alkyl phosphinic acid instead of oleic acid as ligand to grow phase-stable cubic perovskite NCs [11]. Luo's et al. group chose branched capping ligands as passivators and stabilisers for perovskite NCs [12]. Compared to the approaches based on the protective coatings and different capping ligands, blending with polymers to improve the stability of OHP NCs is much easier to handle [17]. The blends of the $CsPbBr_3$ NCs with the PMMA, PS and PBMA prepared by a one-pot strategy could maintain their quantum

[a]**Minjie Fang and Sihui Huang:** These authors contributed equally to this work.
***Corresponding authors: Chunhua Luo,** Key Laboratory of Polar Materials and Devices, Ministry of Education, Department of Optoelectronic Science and Engineering, East China Normal University, Shanghai 200241, China, e-mail: chluo@ee.ecnu.edu.cn. http://orcid. org/0000 0003 2423 7339; and **Hui Peng,** Key Laboratory of Polar Materials and Devices, Ministry of Education, Department of Optoelectronic Science and Engineering, East China Normal University, Shanghai 200241, China; and Collaborative Innovation Center of Extreme Optics, Shanxi University, Taiyuan, Shanxi 030006, China, e-mail: hpeng@ee.ecnu.edu.cn
Minjie Fang, Sihui Huang, Dong Li, Chunli Jiang, Pei Tian and Hechun Lin: Key Laboratory of Polar Materials and Devices, Ministry of Education, Department of Optoelectronic Science and Engineering, East China Normal University, Shanghai 200241, China
Wenlei Yu: Department of Biomedical Engineering, Wenzhou Medical University, Zhejiang 325035, China

yield for more than 1 month in air [13]. Wang et al. prepared $MAPbBr_3$ NC/polymer composite films through the swelling-deswelling microencapsulation strategy and the resulting films showed ultrahigh stability against water and heat [15]. After boiling the samples in water for 30 min, the photoluminescence quantum yields (PLQYs) of the $MAPbBr_3$/PC and $MAPbBr_3$/PS showed decay rates of only less than 7% and 15%, respectively [15].

Self-healing gels are materials that possess the ability to automatically repair their structure and restore their original functionality [18, 19]. Due to this characteristic, self-healing materials can enhance the durability of devices and lower the cost of repairing the damaged devices, which makes them very attractive option in the fabrication of next-generation smart devices with self-repairing properties. Up to now, a large amount of self-healing materials have been developed and applied in coating, sensors, solar cells, supercapacitor and E-skin [20–23]. Among the multifunctional self-healing gels, luminescent self-healing gels combine the properties of self-healing and luminescence, offering the advantages of versatile shaping and patterning, excellent optical qualities and easy control of the refractive index. These advantages make them excellent candidates for various applications, such as sensing, imaging, fluorescent tags and photovoltaic conversion [19, 22, 24]. For example, the usage of PVA hydrogel embedded with inorganic quantum dots as holographic display medium has been illustrated [19]. The self-healing hydrogel containing Eu-polyoxometalate shows reversible luminescent response to acid and base vapours [24].

Among the different self-healing materials, poly(dimethylsiloxane)-urea (PDMS-urea) copolymers are a group of intrinsic self-healing polymers that have been widely investigated due to their tunable mechanical and self-healing properties [25–27]. This group of self-healing polymers can be synthesised through a simple on-step reaction, thus holding great promise for preparing self-healing composites with perovskite NCs. In the current work, we present the preparation of stretchable and self-healing polymer gels with high photoluminescence stability by embedding OHP NCs ($CH_3NH_3PbBr_3$ and $CH_3NH_3PbI_3$) in the PDMS-urea copolymer. The prepared luminescent composite gels are very flexible and stretchable, and show excellent self-healing capability to external damage. Furthermore, the stability of OHP NCs are greatly improved due to the protection of the hydrophobic gel. To the best of our knowledge, this is the first report on self-healable and luminescent polymer gels based on OHP NCs.

2 Experiments

2.1 Synthesis of the PDMS segmented urea copolymer

PDMS-urea was synthesised according to the previously reported method [28, 29]. To a deoxygenated, anhydrous solution of tolylene-2,4-diisocyanate (0.17 g, 1.0 mmol, Sigma-Aldrich, USA) in dried toluene (5.0 ml), PDMS-NH_2 ($M_n = 2500$, 2.6 ml, 1.0 mmol, TCI, Japan) was added, and the mixed solution was stirred for 24 h under nitrogen atmosphere. The resulting viscous solution was stored under nitrogen until further use.

2.2 Synthesis of OHP NCs

For a typical synthesis of $CH_3NH_3PbBr_3$ ($MAPbBr_3$) NCs [30], 0.2 mmol of CH_3NH_3Br (laboratory synthesised), 0.2 mmol of $PbBr_2$ (Aladdin, China), 1 ml of oleic acid (OA, Aladdin, China) and 40 µl of 1-octylamine (OTAm, Aladdin, China) were dissolved in 10 ml of DMF under magnetic stirring at room temperature to form a clear precursor solution. Then, 1.8 ml of the precursor solution was injected into 30 ml of toluene under vigorous magnetic stirring and kept stirring for 10 s to give a green colloid solution. Next, 5 ml of the colloid solution was centrifuged (10 min, 8000 rpm/min) and the NCs that settled on the bottom of the tube were collected and redisposed in 5 ml toluene for the ultraviolet–visible spectroscopy (UV-Vis), photoluminescence (PL), X-ray diffraction (XRD) and transmission electron microscope (TEM) characterisation.

The $CH_3NH_3PbI_3$ ($MAPbI_3$) NCs were synthesised according to the previous reported methods with some modifications [31, 32]. The precursor solution was prepared by dissolving PbI_2 (0.09 mmol, Aladdin, China), CH_3NH_3I (0.1 mmol, laboratory synthesised) and OTAm (20 µl, Aladdin, China) in 200 µl of DMF and 6.8 mL of acetonitrile. The precursor solution was added dropwise into 10 ml of toluene containing 200 µl oleic acid under vigorous stirring. The precipitates were collected by centrifugation using the same method as $MAPbBr_3$ NCs and collected for further use.

2.3 Preparation of the OHP NC/PDMS-urea composites

A certain amount of OHP NCs ($MAPbBr_3$ or $MAPbI_3$) was blended with 1 ml of PDMS-urea solution under stirring

for 10 min to give a uniform solution. The resulting solution was casted onto a home-made Teflon mould. The solvent was evaporated under ambient conditions to form OHP NC/PDMS-urea gels, and the gels were further dried in a vacuum oven at room temperature for 30 min. For the $MAPbBr_3$/PDMS-urea gels, $MAPbBr_3$ NCs loading ratios were changed from 0.4 and 0.8 wt.% to 1.2 wt.%. For the $MAPbI_3$/PDMS-urea gel, only a 0.8 wt.% $MAPbI_3$ NCs loading ratio was used. A blank PDMS-urea gel was also prepared for comparison. The OHP NC/PDMS-urea gels used for UV-Vis and PL characterisation have a thickness of 0.8 mm and width and length of 15 mm. The gel samples used for tensile test have a cylindrical shape with diameter of 3 mm and length of 20 mm.

2.4 Self-healing of the OHP NC/PDMS-urea composite gels

For the self-healing study, the blank copolymer and the composite films containing different OHP NCs contents with dimensions of $15 \times 15 \times 0.8$ mm (length × width × thickness) were used. The films were placed on a glass substrate and cut using a knife. Then, the damaged samples were kept in ambient conditions or at elevated temperatures and the self-healing process was monitored. The PL spectra for self-healing analysis were taken from the self-healing region.

2.5 Characterisation

The UV-vis absorption and photoluminescence spectra were collected using a TU 1901 (Persee, China) and a PerkinElmer LS 55 (Perkinelmer, USA) fluorescence spectrofluorimeter, respectively. The morphology of the $MAPbBr_3$ NCs was characterised on a transmission electron microscope (JEM-2100F, Jeol, Japan). The XRD patterns of the OHP NCs and the OHP NC/PDMS-urea composites were recorded on a Brucker AXS D8 (Brucker, Germany) powder diffractometer using Cu Ka radiation ($l = 0.154$ nm). The absolute photoluminescence quantum yields were determined using a fluorescence spectrometer with an integrated sphere (HORIBA FluroMax-4 spectrofluorimeter, USA) excited at a wavelength of 450 nm. Tensile measurements were performed at 25 °C with an HY-0580 (Hengyi, China) instrument. The molecular weight of the PDMS-urea was determined using Malvern Viscotek GPC Max System (Malvern, USA) with a refractive index detector, a 270 Dual Detector (light scattering and viscometer), and G + T6000M column at 35°C. Tetrahydrofuran (THF) was used as the eluting solvent with a flow rate of 1.0 ml min^{-1}. The system was calibrated with a polystyrene standard. The copolymer solution was filtered through a 0.22-μm poly(vinylidene fluoride) millipore filter before injection. The thermogravimetric analysis (TGA) measurements were performed on a Mettlertoledostar TGA/SDTA851e (Mettler Toledo Star, China) thermogravimetric analyser under a nitrogen atmosphere with a heating rate of 10°C/min.

3 Results and discussion

The PDMS-urea copolymer was synthesised from the $PDMS\text{-}NH_2$ and tolylene-2,4-diisocyanate (TDI) according to the published method [28, 29], as shown in Scheme 1A. After the reaction, the viscous solution was casted onto a Telfon mould and further dried in an vacuum oven for 30 min. The resulting copolymer is colourless and transparent. The measured number-average molecular weight of the copolymer is 13,500 with the polydispersity index of 1.98. Additionally, the PDMS-urea copolymer contains a large amount of urea units, enabling the formation of reversible hydrogen bonds between the polymer backbones (Scheme 1B), resulting in the copolymer flexibility and self-healing capability.

The $CH_3NH_3PbBr_3$ ($MAPbBr_3$) NCs were synthesised by using the solvent-induced re-precipitation method with some modification [30]. The obtained $MAPbBr_3$ NCs are nanoparticles with sizes ranging from 5 nm to 12 nm, based on the TEM (Jeol, Japan) characterisation (Figure 1A). The clear interference fringes from the lattice plane presented in the HRTEM image (the inset in Figure 1A) illustrate the good crystalline order of the prepared $MAPbBr_3$ NCs. Figure 1B presents the UV-Vis absorption and PL spectra of the $MAPbBr_3$ NCs dispersed in toluene. The UV-Vis spectrum shows an absorption onset at 540 nm and a narrow emission peak at 520 nm with a full-width at half-maximum (FWHM) of 26 nm observed in the PL spectrum. The PLQY of the prepared $MAPbBr_3$ NCs is 40%, as measured with an excitation wavelength of 450 nm.

The luminescent $MAPbBr_3$/PDMS-urea gels were prepared by dispersing the collected $MAPbBr_3$ NCs into the PDMS-urea solution in toluene (Scheme 1C). Figure 1C gives the UV-Vis and PL spectra of the $MAPbBr_3$/PDMS-urea gel containing 0.8 wt.% of the $MAPbBr_3$ NCs. A sharper absorption onset at 532 nm is observed for the $MAPbBr_3$ NCs embedded in the polymer gel. The emission peak of the gel is located at 535 nm with a FWHM of 25 nm, which is red-shifted about 15 nm compared to

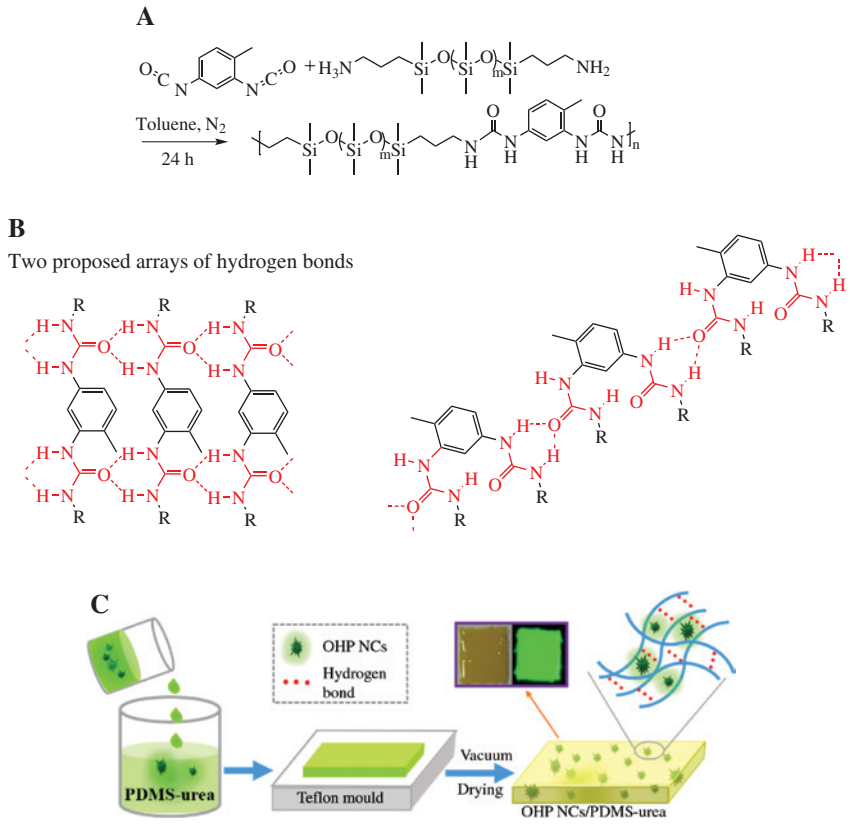

Scheme 1: (A) Synthesis of the PDMS-urea copolymer; (B) Proposed arrays of hydrogen bonding of the PDMS-urea copolymer and (C) Schematic illustration of the preparation and structure of the OHP NC/PDMS-urea gels.

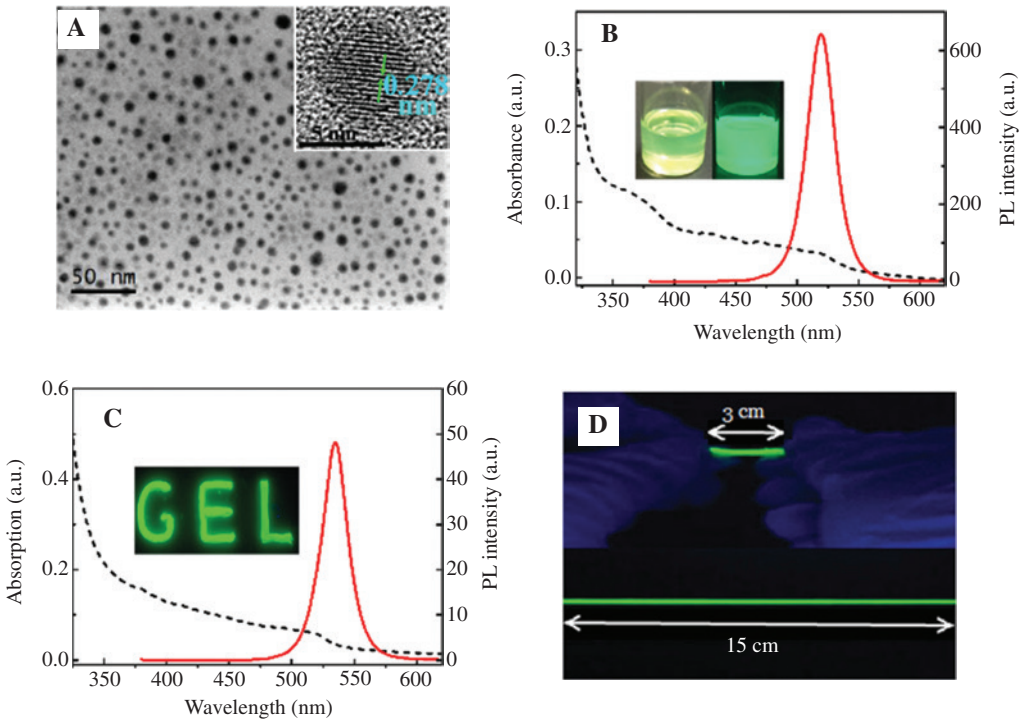

Figure 1: (A) The TEM image of the $MAPbBr_3$ NCs. Inset: the HRTEM image; (B) UV-Vis absorption and PL spectra of the $MAPbBr_3$ NCs dispersed in toluene, Inset: photographs of the solutions for the $MAPbBr_3$ NCs under ambient light and UV light of 365 nm; (C) UV-Vis absorption and PL spectra of the $MAPbBr_3$ (0.8 wt.%)/PDMS-urea gel, Inset: Photograph of the $MAPbBr_3$ (0.8 wt.%)/PDMS-urea gel under UV light of 365 nm and (D) Photograph of the stretched $MAPbBr_3$ (0.8 wt.%)/PDMS-urea taken under 365 nm UV light.

that of $MAPbBr_3$ NCs dispersed in toluene. These results indicate that Ostwald ripening occurred and led to the narrower size distribution of NCs during the gel formation process. The imine groups contained in the polymer chain may contribute to the size optimisation due to the weak coordination between the nitrogen and the lead atoms. The measured PL quantum yield (PLQY) of this gel is 23.8%, which is lower than that of the $MAPbBr_3$ NC solution due to the entrapment of the latter in the solid matrix. The gels containing 0.4 and 1.2 wt.% of $MAPbBr_3$ NCs were also prepared to investigate the effect of the NCs content on the gel's optical properties (Figure S1). Clearly, the PL intensity of the gels first increases with the increase of the $MAPbBr_3$ NCs content. When the content reaches 1.2 wt.%, the PL intensity decreases due to the aggregation of the NCs. On the other hand, the increase of the $MAPbBr_3$ NCs content causes a continuous red-shift of the emission wavelength.

The $MAPbBr_3$/PDMS-urea gel is not only luminescent and flexible, but also presents excellent stretchability. Figure 1D shows that the gel with a length of 3 cm can be stretched up to 15 cm, or up to 500% of its original length, without breaking. To further examine the mechanical property of the gels, tensile tests were performed at room temperature. The corresponding stress-strain curves for the gels with different $MAPbBr_3$ NCs loading ratios of 0.4, 0.8 and 1.2 wt.% are shown in Figure S3. As can be clearly seen, increasing the loading ratio of the $MAPbBr_3$ NCs enhances the tensile strength of the $MAPbBr_3$/PDMS-urea gel while also decreases the elongation of the gel until it breaks. Compared to the blank PDMS-urea gel, the addition of the $MAPbBr_3$ NCs improves the stress tolerance of the gel although it also weakens its extensibility. Additionally, the luminescent $MAPbBr_3$/PDMS-urea gels are relatively transparent. The gel film containing 0.4 wt.% of $MAPbBr_3$ NCs with a thickness of 0.8 mm displays 89% light transmittance over the visible to near-IR region (Figure S4).

XRD measurements were carried out to investigate the effect of the gel formation on the crystal structure of the $MAPbBr_3$ NCs. As shown in Figure 2A, the XRD patterns of the $MAPbBr_3$ NCs, respectively show the characteristic diffraction peaks of cubic $MAPbBr_3$ at 14.9°, 30.1°, 33.8°, 43.2° and 45.8°. The broad peaks at 12.1° and 21.2° observed in the PDMS-urea copolymer reveal the amorphous nature of the PDMS-urea copolymer, which is beneficial to the flexibility and self-healing capability [33]. The characteristic peaks of the $MAPbBr_3$ NCs become more obvious with the increasing $MAPbBr_3$ NCs concentration for the composite gels. The peak locations are the same as those of the $MAPbBr_3$ NCs, thus illustrating no phase change of $MAPbBr_3$ NCs after the gel formation. On the contrary, the broad peak at 12.1° decreases with the increase in the loading ratio of the $MAPbBr_3$ NCs, which could be due to the decline in the order packing of the polymer chain with the addition of $MAPbBr_3$ NCs.

The Fourier-transform infrared (FTIR) analysis (Figure 2B) was also performed to investigate the interaction of the $MAPbBr_3$ NCs with the PDMS-urea polymer molecules. The PDMS-urea polymers exhibit three peaks at 1565, 1640 and 3325 cm^{-1}, which are assigned to the –NH–CO– (amide), –C=O (carbonyl) and N–H stretching vibrations of the urea groups, respectively [34, 35]. Compared to the frequencies of the free N–H (3445–3450 cm^{-1}) and –C=O (1690–1700 cm^{-1}) bands, the observed frequency shifts of the N–H and –C=O bands indicate the formation of strong hydrogen bonds between the urea groups [34, 35]. The FTIR spectra of the composite gels

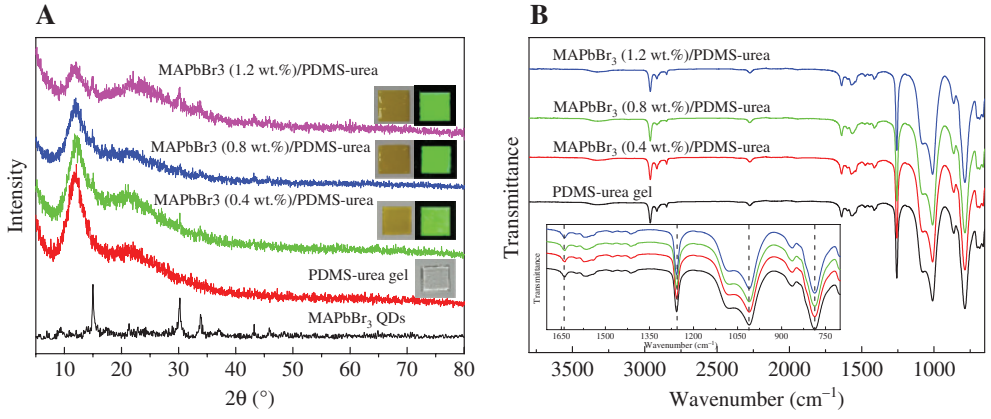

Figure 2: (A) XRD patterns of the $MAPbBr_3$ QDs, PDMS-urea gel and $MAPbBr_3$/PDMS-urea gels with different loading ratios of the $MAPbBr_3$ QDs and (B) the FTIR spectra of the PDMS-urea gel and MAPbBr3/PDMS-urea composites with different loading ratios of the MAPbBr3 QDs. Inset: enlarged FTIR spectra in the wavenumber range of 1680–600 cm^{-1}.

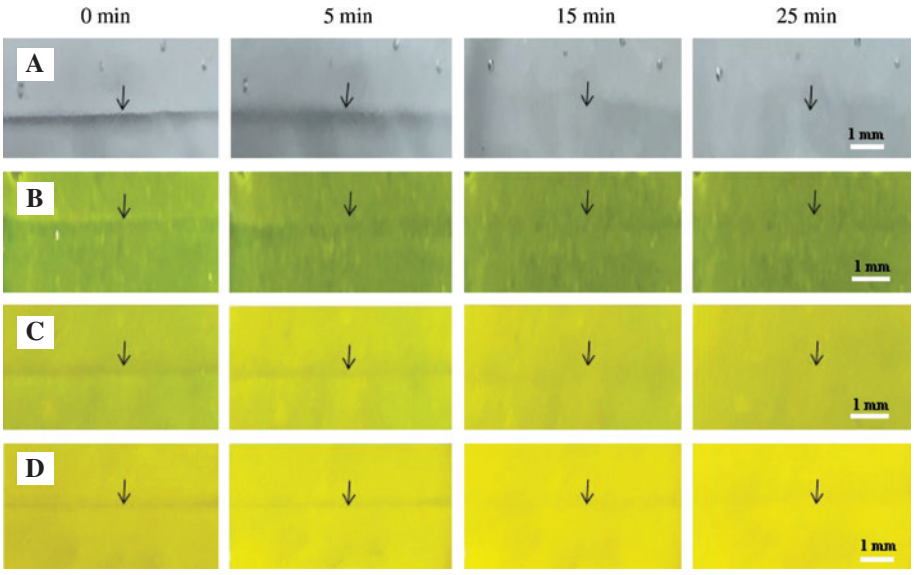

Figure 3: The process of self-healing for the $MAPbBr_3$/PDMS-urea composite films with different perovskite QDs loading. (A) PDMS-urea gel; (B) $MAPbBr_3$ (0.4 wt.%)/PDMS-urea; (C) $MAPbBr_3$ (0.8 wt.%)/PDMS-urea and (D) $MAPbBr_3$ (1.2 wt.%)/PDMS-urea.

are very similar to that of the PDMS-urea copolymer, and no significant changes are observed in the relative band intensities. These results reveal that the embedding of the $MAPbBr_3$ NCs in the PDMS-urea copolymer does not interfere with the formation of hydrogen bonds between the polymer chains, which is crucial for maintaining the self-healing capability of the PDMS-urea copolymer. The thermostability of the gels was characterised by the TGA measurements (Figure S5). The TGA curves show initial weight losses of about 1.1% and 1.0% between 116°C–245°C and 153°C–240°C for the blank PDMS-urea gel and the $MAPbBr_3$ (0.8 wt. %)/PDMS-urea gel, respectively. These initial weight losses should correspond to the evaporation of the solvents. The degradation between 240°C and

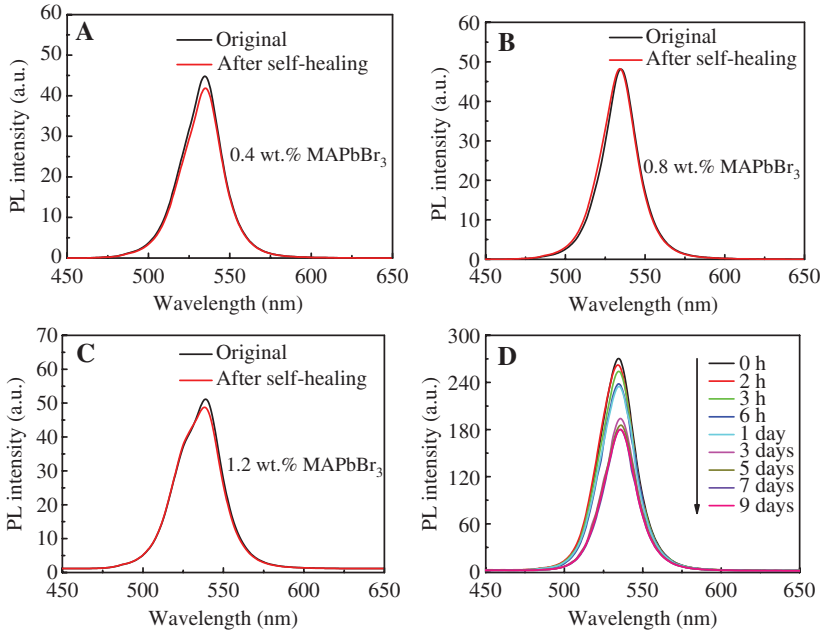

Figure 4: The PL spectra of $MAPbBr_3$/PDMS-urea gels with different $MAPbBr_3$ NC loading ratios before and after self-healing. (A) 0.4 wt.% of $MAPbBr_3$ NCs; (B) 0.8 wt.% of $MAPbBr_3$ NCs and (C) 1.2 wt.% of $MAPbBr_3$ NCs. (D) Evaluation of the PL stability of the $MAPbBr_3$ (0.8 wt.%)/PDMS-urea gel by immersing the gel into water at room temperature.

440°C is attributed to decomposition of the urea bonds and the soft PDMS segments, followed by the carbonisation of the aromatic unit of the TDI between 440°C and 600°C [36]. These results indicate the considerably good thermostability of the gel.

The reversibility of the hydrogen bond presented in the urea unit endows the PDMS-urea gel with great self-healing capability [34]. The influence of the $MAPbBr_3$ NCs on this capability was evaluated by using the blank PDMS-urea copolymer and the composite gels with different $MAPbBr_3$ NCs loadings. The thicknesses of the tested film samples were controlled to be about 0.8 mm by using the Teflon mould. The films were cut by using a knife to make a scratch with a depth of about 0.4 mm. The damaged samples were then kept in ambient conditions, and the self-healing process was monitored. The photographs taken at different times are presented in Figure 3. For all the samples, the scratches completely disappeared 15 min after cutting, implying the full recovery of the gels. Compared to the blank PDMS-urea gel, the self-healing rates of the tested $MAPbBr_3$/PDMS-urea gels show no distinct difference. All these results illustrate that the $MAPbBr_3$ NCs have no obvious influence on the self-healing capability of the PDMS-urea gel in the tested $MAPbBr_3$ NC loading range.

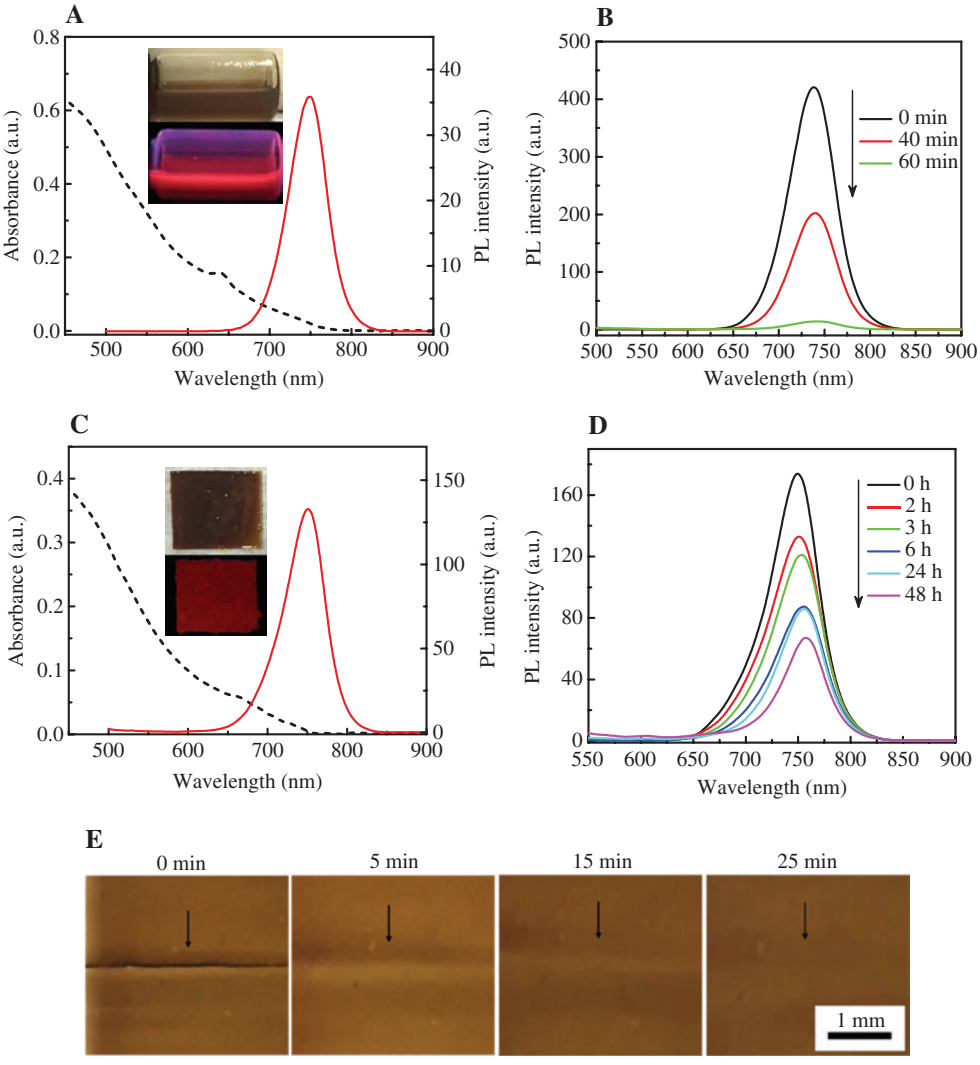

Figure 5: (A) UV-Vis absorption and PL spectra of $MAPbI_3$ NCs dispersed in toluene. Insets: photographs of the $MAPbI_3$ NCs dispersed in toluene under ambient light (top) and UV light of 365 nm (bottom); (B) Evaluation of the PL stability of the $MAPbI_3$ NCs dispersed in toluene after the addition of water at room temperature; (C) UV-Vis absorption and PL spectra of the $MAPbI_3$ (0.8 wt.%)/PDMS-urea gel, Insets: photographs of the $MAPbI_3$ (0.8 wt.%)/PDMS-urea gel under ambient light (top) and UV light of 365 nm (bottom); (D) Evaluation of the PL stability of the $MAPbI_3$ (0.8 wt.%)/PDMS-urea gel immersed in water at room temperature. (E) The self-healing process of the $MAPbI_3$/PDMS-urea gel with 0.8 wt.% $MAPbI_3$ NCs [36].

We further investigated the effect of temperature on the self-healing rate by choosing the $MAPbBr_3$ NC (0.8 wt.%)/PDMS-urea gel as a representative. As depicted in Figure S6, the damaged gel can fully recover within 10 min and 5 min at 40°C and 50°C, respectively. This demonstrates that the higher temperature leads to the faster self-healing rate due to the accelerated movement of polymer molecular segment.

To determine whether the self-healing process affected the PL properties of the $MAPbBr_3$/PDMS-urea gel, the PL spectra were taken from the same region of the samples before cutting and after the self-healing process. The results are given in Figure 4A–C. As can be seen, the PL intensities of the three tested samples show little differences before and after the self-healing process, indicating the good PL stability of the $MAPbBr_3$/PDMS-urea gels.

The $MAPbBr_3$ NCs are quite sensitive to moisture. The PL intensity of the $MAPbBr_3$ NCs dispersed in toluene decreases to 36% of the initial value after the addition of water for 2 h (Figure S7). We investigated the PL stability of the $MAPbBr_3$/PDMS-urea gel by immersing the sample containing 0.8 wt.% of the $MAPbBr_3$ NCs into water at room temperature. Figure 4D presents the changes of PL intensity with time. In the initial 6 h, the PL intensity decreased relatively fast. After 7 days, the PL intensity decayed to 67% of the initial value, and then kept stable. The first decrease of the PL intensity could be due to the degradation of the $MAPbBr_3$ NCs located on the surface of the gel. After the complete decomposition of the $MAPbBr_3$ NCs on the gel surface, the hydrophobic gel prevents the further decomposition of the inner $MAPbBr_3$ NCs, after which the PL intensity remained constant. These results illustrate that the PDMS-urea gel greatly improves the stability of the $MAPbBr_3$ NCs against water.

To illustrate the versatility of our strategy to improve the stability of perovskite NCs, we further synthesised $CH_3NH_3PbI_3$ ($MAPbI_3$) NCs with red emission. The measured XRD spectrum (Figure S8) confirms the tetragonal phase of the $MAPbI_3$ NCs and agrees well with previous reports [31, 32]. Figure 5A gives the UV-Vis absorption and PL spectra of the obtained $MAPbI_3$ NCs dispersed in toluene. The $MAPbI_3$ NCs shows a main absorption peak at 639 nm and the emission peak at 746 nm with a FWHM of 54 nm. The $MAPbI_3$ NCs are more sensitive to water than the $MAPbBr_3$ NCs. Moreover, the PL intensity of the $MAPbI_3$ NCs dispersed in toluene drops very fast to nearly zero within 1 h after the addition of water, as shown in Figure 5B. Compared to the $MAPbI_3$ NCs dispersion in toluene, the absorption and emission peak of $MAPbI_3$/PDMS-urea gel red-shift to 670 and 749 nm (Figure 5C), respectively. The emission peak becomes broad and the FWHM increases to 60 nm. Similar to the $MAPbBr_3$/PDMS-urea gel, the formation of the $MAPbI_3$/PDMS-urea gel greatly improves the PL stability of the $MAPbI_3$ NCs. After immersing the gel into water for 2 h, the PL intensity is only reduced by 27% of its initial value (Figure 5D). After 48 h, the PL intensity still maintains 39% of its initial value. The $MAPbI_3$/PDMS-urea gel also exhibits excellent self-healing capability, as illustrated in Figure 5E. The scratch made by cutting completely disappeared after 15 min, illustrating the full recovery of the gel.

The enhanced PL stability and excellent self-healing capability of the OHP NC/PDMS-urea gels with simple preparation process make them very promising materials for use in many optical systems, such as LEDs, imaging and sensing. To illustrate their capability as phosphors for LEDs, blue GaN LED chips (0.8 watt) were coated with $MAPbBr_3$ (0.8 wt.%)/PDMS-urea and $MAPbI_3$ (0.8 wt.%)/PDMS-urea gels, respectively, as shown in Figure 6A and B, respectively. The emission of the used GaN LED chip is at 458 nm with a FWHM of 21 nm. After coating with the $MAPbBr_3$/PDMS-urea gel, the blue emission of the LED chip is fully converted to green and

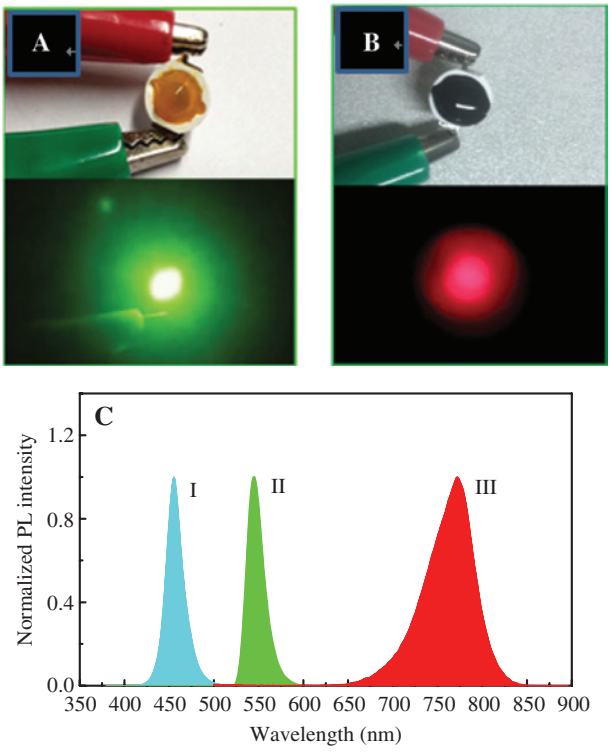

Figure 6: Photographs of (A) the $MAPbBr_3$/PDMS-urea gel and (B) the $MAPbI_3$/PDMS-urea gel-coated GaN LEDs under the operation potential of 2.7 V and (C) Emission spectra of the blue GaN LED (I), the $MAPbBr_3$/PDMS-urea gel coated green LED (II) and the $MAPbI_3$/PDMS-urea gel coated red LED (III).

the emission peak is at 549 nm with a FWHM of 23 nm (Figure 6C). The $MAPbI_3$/PDMS-urea gel can also completely convert the blue emission of the LED chip to red emission.

4 Conclusions

In this work, we have successfully prepared luminescent OHP NC/PDMS-urea gels by a simple process. These gels are flexible, stretchable and relatively transparent. More importantly, the prepared OHP NC/PDMS-urea gels present excellent self-healing capability. Due to the hydrophobic feature of the PDMS-urea copolymer, the stability of the OHP NCs ($MAPbBr_3$ NCs and $MAPbI_3$ NCs) against water is greatly improved after the formation of the composite gels. The use of $MAPbBr_3$/PDMS-urea and $MAPbI_3$/PDMS-urea gels as green and red phosphors for LEDs, respectively, has been successfully demonstrated. Due to the above-mentioned properties, the OHP NC/PDMS-urea polymer composite gels are very promising materials for fabricating next generation smart optical devices with self-healing property.

Acknowledgements: This work was financially supported by the Natural Science Foundation of Shanghai, Funder Id: http://dx.doi.org/10.13039/100007219 (No. 18ZR1410900), the Natural Science Foundation of China, Funder Id: http://dx.doi.org/10.13039/501100001809 (No. 61671206), the China Postdoctoral Science Foundation (No. 2017M621540), the Shanghai Science and Technology Innovation Action Plan (No. 17JC1402500), the Natural Science Foundation of Zhejiang Province, Funder Id: http://dx.doi.org/10.13039/501100004731 (No. LQ16F050005) and by the Science and Technology Bureau of Wenzhou (No. G20150025).

Conflicts of interest: There are no conflicts of interest to declare.

References

[1] Protesescu L, Yakunin S, Bodnarchuk MI, et al. Nanocrystals of cesium lead halide perovskites ($CsPbX_3$, X=Cl, Br, and I): novel optoelectronic materials showing bright emission with wide color gamut. Nano Lett 2016;15:3692–6.
[2] You YM, Liao WQ, Zhao D, et al. An organic-inorganic perovskite ferroelectric with large piezoelectric response. Science 2017;357:306.
[3] Polavarapu L, Nickel B, Feldmann J, Urban Alexander S. Advances in quantum-confined perovskite nanocrystals for optoelectronics. Adv Energy Mater 2017;7:1700267.
[4] Lee MM, Teuscher J, Miyasaka T, Murakami TN, Snaith HJ. Efficient hybrid solar cells based on meso-superstructured organometal halide perovskites. Science 2012;338:643–7.
[5] Xing G, Mathews N, Lim SS, et al. Low-temperature solution-processed wavelength-tunable perovskites for lasing. Nat Mater 2014;13:476–80.
[6] Hintermayr VA, Richter AF, Ehrat F, et al. Tuning the optical properties of perovskite nanoplatelets through composition and thickness by ligand-assisted exfoliation. Adv Mater 2016;28:9478–85.
[7] Snaith HJ. Perovskites: the emergence of a new era for low-cost, high-efficiency solar cells. J Phy Chem Lett 2013;4:3623–30.
[8] Sun H, Yang Z, Wei M, et al. Chemically addressable perovskite nanocrystals for light-emitting applications. Adv Mater 2017;29:1701153.
[9] Chen J, Zhou S, Jin S, Li H, Zhai T. Crystal organometal halide perovskites with promising optoelectronic applications. J Mater Chem C 2016;4:11–27.
[10] Huang S, Li Z, Long K, Zhu N, Shan A, Liang L. Enhancing the stability of CH3NH3PbBr3 quantum dots by embedding in silica spheres derived from tetramethyl orthosilicate in “waterless” toluene. J Am Chem Soc 2016;138:5749.
[11] Wang C, Chesman AS, Jasieniak JJ. Stabilizing the cubic perovskite phase of CsPbI3 nanocrystals by using an alkyl phosphinic acid. Chem Commun 2016;53:232.
[12] Luo B, Pu YC, Lindley SA, et al. Organolead halide perovskite nanocrystals: branched capping ligands control crystal size and stability. Angew Chem Int Ed 2016;128:9010–4.
[13] Xin Y, Zhao H, Zhang J. Highly stable and luminescent perovskite-polymer composites from a convenient and universal Strategy. ACS Appl Mater Inter 2018;10:4971.
[14] Raja SN, Bekenstein Y, Koc MA, et al. Encapsulation of perovskite nanocrystals into macroscale polymer matrices: enhanced stability and polarization. ACS Appl Mater Inter 2016;8:35523–33.
[15] Wang Y, He J, Chen H, et al. Ultrastable, highly luminescent organic-inorganic perovskite-polymer composite films. Adv Mater 2016;28:10710–7.
[16] Chang S, Bai Z, Zhong H. In situ fabricated perovskite nanocrystals: a revolution in optical materials. Adv Opt Mater 2018;6:1800380.
[17] Wang H, Lin H, Piao X, et al. Organometal halide perovskite nanocrystals embedded in silicone resins with bright luminescence and ultrastability. J Mater Chem C 2017;5:12044–9.
[18] Taylor DL; Marc in het Panhuis. Self-healing hydrogels. Adv Mater 2016;28:9060–93.
[19] Zhu M, Zhong H, Jia J, et al. PVA hydrogel embedded with quantum dots: a potential scalable and healable display medium for holographic 3D applications. Adv Opt Mater 2014;2:338–42.
[20] Zhou Q, Bai Z, Lu W-g, Wang Y, Zou B, Zhong H. In situ fabrication of halide perovskite nanocrystal-embedded polymer composite films with enhanced photoluminescence for display backlights. Adv Mater 2016;28:9163–8.
[21] Chen D, Wang D, Yang Y, Huang Q, Zhu S, Zheng Z. Self-healing materials for next-generation energy harvesting and storage devices. Adv Energy Mater 2017;7:1700890.
[22] Mphahlele K, Ray SS, Kolesnikov A. Self-healing polymeric composite material design, failure analysis and future outlook: a review. Polymers 2017;9:535.

[23] Zhang Q, Liu L, Pan C, Li D. Review of recent achievements in self-healing conductive materials and their applications. J Mater Sci 2018;53:27–46.
[24] Yang J, Chen M, Li P, et al. Self-healing hydrogel containing Eu-polyoxometalate as acid-base vapor modulated luminescent switch. Sensors Actuat, B 2018;273:153–8.
[25] Guo K, Zhang DL, Zhang XM, et al. Conductive elastomers with autonomic self-healing properties. Angew Chem Int Ed 2015;54:12127–33.
[26] Cao P-F, Li B, Hong T, et al. Superstretchable, self-healing polymeric elastomers with tunable properties. Adv Funct Mater 2018:1800741.
[27] Riehle N, Thude S, Goetz T, et al. Influence of PDMS molecular weight on transparency and mechanical properties of soft polysiloxane-urea-elastomers for intraocular lens application. Eur Polym J 2018;101:190–201.
[28] Yílgör Ì, Sha'Aban AK, Steckle Jr. WP, Tyagi D, Wilkes GL, Mcgrath JE. Segmented organosiloxane copolymers. 1. Synthesis of siloxane – urea copolymers. Polymer 1984;25:1800–6.
[29] Baek P, Aydemir N, Chaudhary OJ, et al. Polymer electronic composites that heal by solvent vapour. RSC Adv 2016;6:98466–74.
[30] Zhang F, Zhong H, Chen C, et al. Brightly luminescent and color-tunable colloidal CH3NH3PbX3 (X=Br, I, Cl) quantum dots: potential alternatives for display technology. ACS Nano 2015;9:4533–42.
[31] Zhang F, Huang S, Wang P, et al. Colloidal synthesis of air-stable CH3NH3PbI3 quantum dots by gaining chemical insight into the solvent effects. Chem Mater 2017;29:3793–9.
[32] Pathak S, Sakai N, Wisnivesky Rocca Rivarola F, et al. Perovskite crystals for tunable white light emission. Chem Mater 2015;27:8066–75.
[33] Yanagisawa Y, Nan Y, Okuro K, Aida T. Mechanically robust, readily repairable polymers via tailored noncovalent cross-linking. Science 2018;359:72–6.
[34] Huynh T-P, Sonar P, Haick H. Advanced materials for use in soft self-healing devices. Adv Mater 2017;29:1604973.
[35] Yilgor E, Burgaz E, Yurtsever E, Yilgor I. Comparison of hydrogen bonding in polydimethylsiloxane and polyether based urethane and urea copolymers. Polymer 1999;41:849–57.
[36] Chuang FS, Tsen WC, Shu YC. The effect of different siloxane chain-extenders on the thermal degradation and stability of segmented polyurethanes. Polym Degrad Stab 2004;84:69–77.

Supplementary Material: The online version of this article offers supplementary material (https://doi.org/10.1515/nanoph-2018-0126).